ASTRONOMY
AND
ASTROPHYSICS

Solar models and NACRE thermonuclear reaction rates

P. Morel[1], **B. Pichon**[2], **J. Provost**[1], **and G. Berthomieu**[1]

[1] Département Cassini, UMR CNRS 6529, Observatoire de la Côte d'Azur, B.P. 4229, F-06304 Nice Cedex 4, France
[2] DARC, UMR CNRS 8629, Observatoire de Paris Section Meudon, F-92195 Meudon Cedex, France

Abstract. Using the most recent updated physics, calibrated solar models have been computed with the new thermonuclear reaction rates of NACRE, the recently available European compilation. Comparisons with models computed with the reaction rates of Caughlan & Fowler (1988) and of Adelberger et al. (1998) are made for global structure, expected neutrinos fluxes, chemical composition and sound speed profiles, helioseismological properties of p-modes and g-modes.

Key words: nuclear reactions, nucleosynthesis, abundances – Sun: evolution – Sun: interior – Sun: oscillations

1. Introduction

Precise solar models have been constructed over the past three and a half decades (see, e.g. Bahcall et al. 1963; Bahcall 1993, Bahcall et al. 1998b). Refinements of these models have accelerated in the past decade (see, e.g. Bahcall & Ulrich 1988, Bahcall & Pinsonneault 1992b). For ten years many stellar and solar models have been computed using the thermonuclear reaction rates of Caughlan & Fowler (1988, hereafter C88), a popular compilation but not optimized for solar conditions. More recently, some authors (e.g. Bahcall et al. 1995; Reiter et al. 1995; Chaboyer et al. 1995; Berthomieu et al. 1995; Christensen-Dalsgaard et al. 1996) employed the improved thermonuclear reaction rates adopted by Bahcall & Pinsonneault (1992a) for the calculation of accurate solar models. Meanwhile several groups of nuclear physicists have made other compilations of updated thermonuclear reaction rates of astrophysical interest. A year ago the compilation of Adelberger et al. (1998, hereafter A98) was published. The original motivation of this compilation is to assess the state of the nuclear physics important to the solar neutrino problem. The incidences on solar models of these new reaction rates have been analyzed by several groups (see e.g. Bahcall et al. 1998b; Brun et al. 1998; Morel et al. 1998). More recently the European Nuclear Astrophysics Compilation of Reaction rates (Angulo et al. 1999, NACRE, hereafter N99) has been completed and opened to free access. The driving motivation of this last work, coordinated by the Institut d'Astronomie

et d'Astrophysique of the Université Libre de Bruxelles, is the build-up of well documented and evaluated sets of experimental data or theoretical predictions of astrophysical interest. To have a direct idea of the degree of reliability of any reaction rate, the authors have published, both a very convenient plot of the available measurements of cross section S-factors with respect to energy, as well as a table showing the range of the various parameters needed for cross section evaluation, e.g. the resonance parameters. Moreover, the accuracy of each analytical fit is indicated. This new compilation gives, besides the adopted reaction rate $\mathcal{R}$, its lower and upper limits $\mathcal{R}_l$ and $\mathcal{R}_u$. A solar neutrino analysis based on preliminary NACRE data for the PP reactions has been done by Castellani et al. (1997). Recently Arnould et al. (1999) have used the N99 reaction rates to compute abundance predictions in non explosive hydrogen and helium burning. They convincingly show that large spreads in the abundances predictions for several nuclides may result not only from a change in temperature, but also from nuclear physics uncertainties.

We are now in the fortunate position of having two precise and *independent* determinations of the best nuclear fusion data, namely A98 and N99. In order to illustrate the effects, on the standard solar model, of nuclear fusion rates on various astronomical quantities, including neutrino fluxes and helioseismology frequencies, we compare the model results calculated with the best current data from A98 and N99, with results obtained using early estimates of fusion rates of C88. Those differences are not very large. Nevertheless they modify the energy balance, the stratification, the chemical composition and the neutrino generation in the core.

Let us first recall the main constraints known nowadays on solar models. The helioseismological constraints relevant to the core are the small p-mode frequency differences $\delta\nu_{02}$ and $\delta\nu_{13}$ and the not yet observed spectrum of gravity modes. Other signatures of changes of thermonuclear reaction rates will be the sound velocity profile which is known from inversion of helioseismic data between $R \gtrsim 0.1\,R_\odot$ and $R \lesssim 0.9\,R_\odot$, and also the radius of the base of the solar convection zone which is precisely located. The number of observed photospheric depletions of lithium and beryllium which are often ascribed to transport phenomena beneath the convection zone are also sensitive to changes of the thermonuclear reaction rates in their low energy

Table 1. Respectively for the C88, A98 and N99 compilations, the S-factors at zero energy S(0) (MeV barn) and S'(0) (barn) are given for each nuclear reaction of solar interest, but $^7\text{Be}(e^-, \nu_{7\text{Be}}\gamma)^7\text{Li}$. The last column gives $\Delta\mathcal{R}$, the global uncertainty of N99's rates computed, for $T_6 = 15$, according to Eq. 1. The S(0) factor of $^{12}\text{C}(p,\gamma)^{13}\text{N}$ is estimated from the N99 plot.

reactions	C88 S(0)	C88 S'(0)	A98 S(0)	A98 S'(0)	N99 S(0)	N99 S'(0)	$\Delta\mathcal{R}$
$^1\text{H}(p,\beta^+\nu_{\text{pp}})^2\text{H}$	$4.06\,10^{-25}$	$4.6\,10^{-24}$	$4.00\,10^{-25}$	$4.48\,10^{-24}$	$3.94\,10^{-25}$	$4.61\,10^{-24}$	5%
$^2\text{H}(p,\gamma)^3\text{He}$	$2.5\,10^{-7}$	$7.9\,10^{-6}$			$2.0\,10^{-7}$	$5.6\,10^{-6}$	40%
$^3\text{He}(^3\text{He},2p)^4\text{He}$	5.56	-8.2	5.4	-4.1	5.18	-2.22	6%
$^3\text{He}(\alpha,\gamma)^7\text{Be}$			$5.3\,10^{-4}$	$-3.0\,10^{-4}$	$5.4\,10^{-4}$	$-5.2\,10^{-4}$	18%
$^7\text{Li}(p,\alpha)^4\text{He}$					$5.93\,10^{-2}$	0.193	14%
$^7\text{Be}(p,\gamma)^8\text{B}^*$	$2.39\,10^{-5}$	0.	$1.9\,10^{-5}$	$-1.35\,10^{-5}$	$2.1\,10^{-5}$	$-1.8\,10^{-5}$	11%
$^{12}\text{C}(p,\gamma)^{13}\text{N}$	$1.40\,10^{-3}$	$4.2\,10^{-3}$	$1.34\,10^{-3}$	$2.6\,10^{-3}$	$1.5\,10^{-3}$		11%
$^{13}\text{C}(p,\gamma)^{14}\text{N}$	$5.5\,10^{-3}$	$1.3\,10^{-2}$	$7.6\,10^{-3}$	$-7.8\,10^{-3}$	$7.0\,10^{-3}$		23%
$^{14}\text{N}(p,\gamma)^{15}\text{O}$	$3.2\,10^{-3}$	$-5.7\,10^{-3}$	$3.5\,10^{-3}$	$-1.28\,10^{-2}$	$3.2\,10^{-3}$		34%
$^{15}\text{N}(p,\gamma)^{16}\text{O}$	$6.4\,10^{-2}$	$3.2\,10^{-2}$	$6.4\,10^{-2}$	$2.1\,10^{-2}$	$6.4\,10^{-2}$		23%
$^{15}\text{N}(p,\alpha)^{12}\text{C}$	71.	423.	67.5	310.	69.		15%
$^{16}\text{O}(p,\gamma)^{17}\text{F}$	$9.3\,10^{-3}$		$9.4\,10^{-3}$	$-2.4\,10^{-2}$	$9.3\,10^{-3}$		36%
$^{17}\text{O}(p,\alpha)^{14}\text{N}$			$9.58\,10^{-4}$	$1.08\,10^{-2}$			35%

regime. Another constraint also connected to nuclear reaction rates is the isotopic ratio $^3\text{He}\,/\,^4\text{He}$ measured currently at the solar surface which is sensitive to the pre-main sequence deuteron burning and to initial isotopic ratios $^2\text{H}\,/\,^1\text{H}$ and $^3\text{He}\,/\,^4\text{He}$ of cosmological interest.

The paper is organized as follows: in Sect. 2 in the low energy range, for the nuclear reactions of interest for solar modeling, we summarize the main differences between N99 and A98 with respect to C88. The physics used in the models is described in Sect. 3. In Sect. 4 we report results of comparisons between calibrated solar models computed with N99, A98 and C88, finally we conclude in Sect. 5.

2. Comparison of thermonuclear reaction rates from N99, A98 and C88 compilations

The most important nuclear reactions relevant for solar modeling are, for the PP chains (Clayton 1968; Bahcall 1989 Tables. 3.1 and 3.3):

$^1\text{H}(p,\beta^+\nu_{\text{pp}})^2\text{H}$, $^2\text{H}(p,\gamma)^3\text{He}$, $^3\text{He}(^3\text{He},2p)^4\text{He}$,
$^3\text{He}(\alpha,\gamma)^7\text{Be}$, $^7\text{Be}(e^-,\nu_{7\text{Be}}\gamma)^7\text{Li}$, $^7\text{Li}(p,\alpha)^4\text{He}$,
$^7\text{Be}(p,\gamma)^8\text{B}^*(\beta^+\nu_{8\text{B}})^8\text{Be}(\alpha)^4\text{He}$,

and for the CNO bi-cycle:

$^{12}\text{C}(p,\gamma)^{13}\text{N}(\beta^+\nu_{13\text{N}})^{13}\text{C}$, $^{13}\text{C}(p,\gamma)^{14}\text{N}$,
$^{14}\text{N}(p,\gamma)^{15}\text{O}(\beta^+\nu_{15\text{O}})^{15}\text{N}$, $^{15}\text{N}(p,\gamma)^{16}\text{O}$, $^{15}\text{N}(p,\alpha)^{12}\text{C}$,
$^{16}\text{O}(p,\gamma)^{17}\text{F}(\beta^+\nu_{17\text{F}})^{17}\text{O}$, $^{17}\text{O}(p,\alpha)^{14}\text{N}$.

Owing to their low termination and small contribution to energetic and nucleosynthesis, despite their interest for neutrino generation, we do not explicitly take into account in the nuclear network $^1\text{H}(pe^-,\nu_{\text{pep}})^2\text{H}$ and $^3\text{He}(p,e^+\nu_{\text{hep}})^4\text{He}$ the so-called *pep* and *hep* reactions. Nevertheless we compute the number

of ν_{pep} neutrino generated using the Eq. (3.17) of the Bahcall's (1989) reference text book.

The changes between the reaction rates of N99, A98 and C88 are extensively commented in Adelberger et al. (1998) and Angulo et al. (1999). As a matter of illustrations, for the three compilations and for each PP and CNO reaction – but the electronic capture $^7\text{Be}(e^-,\nu_{7\text{Be}}\gamma)^7\text{Li}$ – Table 1 gives the S-factors at zero energy and the underlying global uncertainty on the rate $\Delta\mathcal{R}$:

$$\Delta\mathcal{R} = \sqrt{\frac{\mathcal{R}_\text{u}}{\mathcal{R}_\text{l}}} - 1, \tag{1}$$

estimated for $T_6 = 15$; T_6 is the temperature in M K, $\mathcal{R}_\text{l}$ (*resp.* $\mathcal{R}_\text{u}$) stands for lower (*resp.* upper) limit of N99 updated reaction rates. For our thermonuclear reaction network the contributions of resonances to the astrophysical reaction rates are negligible in the solar range of temperatures, therefore the values of S(0) and, if any, S'(0), presented here, are pertinent. For sake of brevity we have not reproduced the known S''(0) values. Fig. 1 (*resp.* Fig. 2) compares the relative differences between the adopted rates of N99 (*resp.* A98) and C88 for the temperature range $0.5 \leq T_6 \leq 19$.

We next briefly recall the main changes in the rates of A98 and N99, with respect to those of C88 which is the oldest and, up to now, the most used and complete.

$^2\text{H}(p,\gamma)^3\text{He}$: Among all reactions of PP chains and CNO bi-cycle, it is the rate of this PPI reaction which is the least known. The reaction rate is so fast that it is only involved by the pre-main sequence deuteron burning. Owing to the lower value adopted for the S-factors at zero energy, the rate of the reaction which synthesizes ^3He is about -24% lower in N99 than in C88. This reaction is not updated in A98, for the calculations with A98 we used the value adopted in C88.
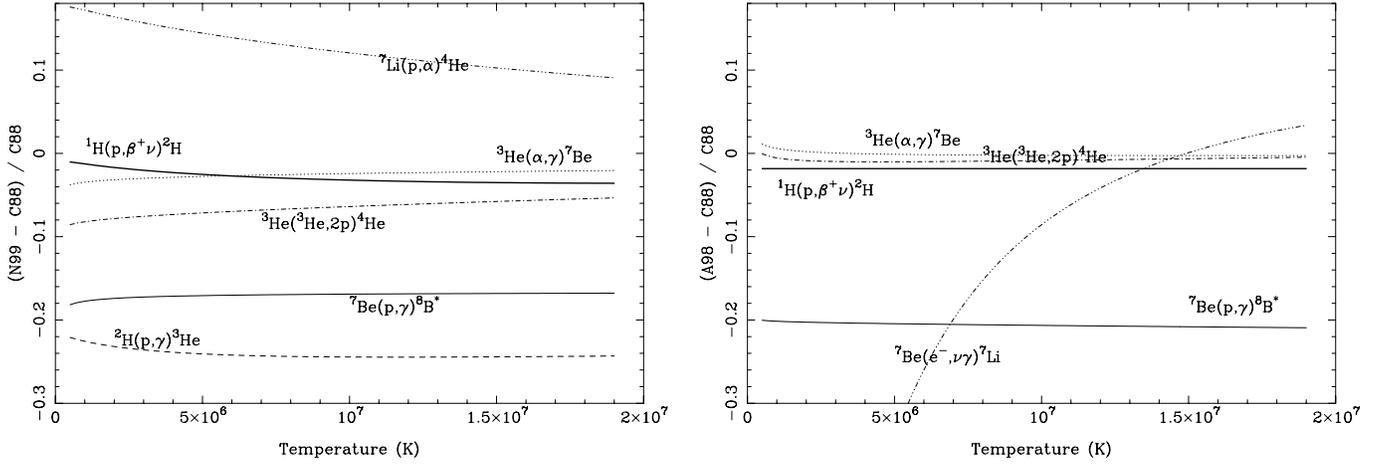
Fig. 1. Left panel: relative differences between the reaction rates between N99 and C88 for the relevant solar temperature range $0.5 \leq T_6 \leq 19$. for the PP reactions: ^{1}H$(p, \beta^+ \nu_{\rm pp})^2$H (heavy, full), ^{2}H$(p, \gamma)^3$He (dashed), ^{3}He$(^3$He, $2p)^4$He (dot-dash-dot-dash), ^{3}He$(\alpha, \gamma)^7$Be (dotted), ^{7}Li$(p, \alpha)^4$He(dash-dot-dot-dot) and ^{7}Be$(p, \gamma)^8$B* (thin, full). Right panel: same between A98 and C88.
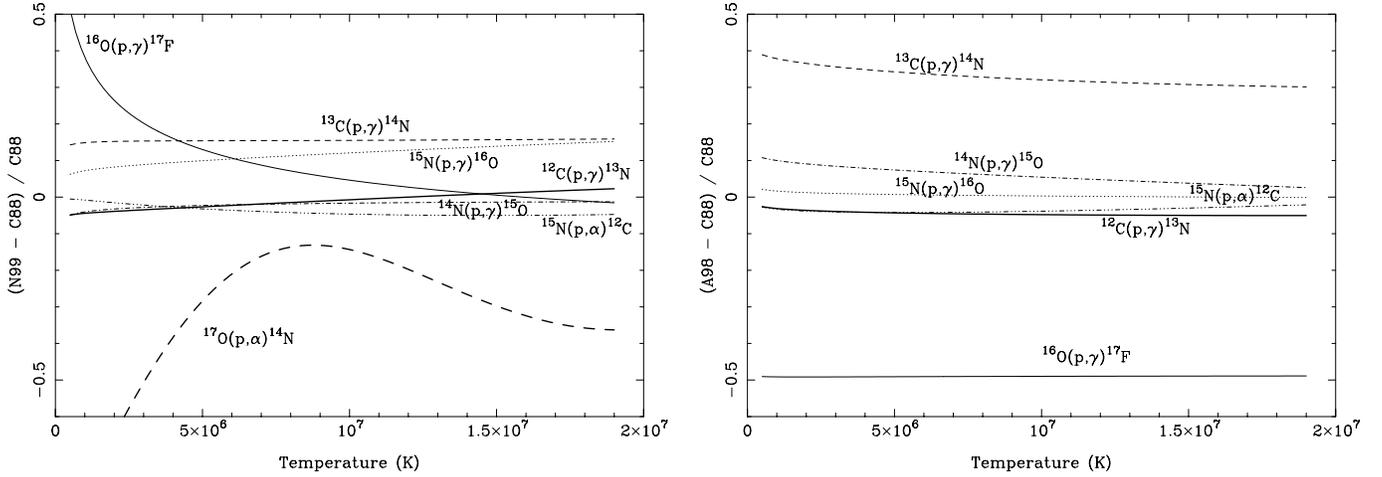
Fig. 2. The same as Fig. 1 for the CNO reactions: ^{12}C$(p, \gamma)^{13}$N (heavy, full), ^{13}C$(p, \gamma)^{14}$N (dashed), ^{14}N$(p, \gamma)^{15}$O (dot-dash-dot-dash), ^{15}N$(p, \gamma)^{16}$O (dotted), ^{15}N$(p, \alpha)^{12}$C (dash-dot-dot-dot), ^{16}O$(p, \gamma)^{17}$F (thin, full), ^{17}O$(p, \alpha)^{14}$N (heavy, dashed).

^{3}He$(^3$He, $2p)^4$He: For the most energetic reaction of the PP chains N99 (*resp.* A98) adopts values smaller by about -6% (*resp.* -2%) than C88 for the S-factors. As a consequence of the calibration process, for the models using either N99 or A98, more ^{1}H nuclear fuel will be burnt in order to reach, the currently observed luminosity and effective temperature. Therefore these models will have cores with larger temperature, helium content, density and sound velocity than models computed with C88; then, at first sight, their predicted total neutrino fluxes are expected to be larger. This effect will be enhanced for the models computed with N99 since the rates of the two reactions ^{1}H$(p, \beta^+ \nu_{\rm pp})^2$H and ^{2}H$(p, \gamma)^3$He are smaller in N99 than in C88.

For that reaction, the plot of the available measurements of cross section S-factors given by Angulo et al. (1999), gives the impression that, at low energy, the Junker at al.'s (1998) recent measurements are avoided by the interpolation formulae adopted (see also Fig. 2 of Adelberger et al. 1998). These recent data should lead to an increase of S(0) so, to an enhancement of the efficiency of the reaction and then, owing to the calibration process, to a decrease of solar neutrino fluxes.

^{7}Li$(p, \alpha)^4$He: The S(0) value adopted by N99 differs from C88 between $+15\%$ and $+7\%$. In the core its curate rate is irrelevant due, first to its strong rate ($\approx 10^{-5}$ year, e.g. Bahcall 1989 Table 3.2) and, second to the tiny mass fraction of ^{7}Li $\sim 2\,10^{-15}$. Beneath the convection zone, the burning of ^{7}Li will be more efficient with N99 than with C88, leading to an increase of the lithium depletion at the solar surface now. As suggested in C88, the ^{7}Li burning is slightly enhanced by few percents by the neighbor reaction ^{7}Li$(p, \gamma)^8$Be$(\alpha)^4$He which has been added to our nuclear network. This reaction is not updated in A98. For the calculations with A98 we shall use the value adopted in C88.

^{7}Be$(e^-, \nu_{7_{\rm Be}}\gamma)^7$Li: N99 deals only with charged particle induced reactions involving nuclei, and therefore the ^{7}Be electron capture rate is not updated. In the calculations with N99 we shall used the value given by A98. Beneath $T_6 = 1$ only an upper

limit is given in C88 for the ^{7}Be electron capture. The adopted rate of A98 differs from the rate of C88 by more than $+50\%$ at low temperature; for $T_6 \sim 15$, i.e. in the solar core, the rates of C88 and A98 are of same order.

^{7}Be$(p,\gamma)^8$B*: This reaction controls the efficiency of the important source of ν_{8_B}, the so-called boron solar neutrino. The adopted values for the S-factors at zero energy are slightly larger in N99 than in A98, but still smaller than in C88. With respect to C88, everything else equal, one can expect that the neutrino flux from boron will be *reduced* for the solar models computed with A98 and N99.

^{13}C$(p,\gamma)^{14}$N: The values of S-factors at zero energy adopted by N99 and A98 are magnified by a factor of about two with respect to their previous values in C88; as a result the rates are increased by $+30\%$ and $+15\%$ respectively. These large differences will not have any noticeable incidence on the global structure of the core since the energy generated by the CNO bi-cycle is only $\lesssim 2\%$ of the total nuclear energy.

^{14}N$(p,\gamma)^{15}$O: The rate of the most important reaction for the computation of energy generation and neutrino fluxes created by the CNO bi-cycle is known with a large uncertainty. The three compilations adopt about the same values for the S-factors at zero energy. Fig. 2 shows small differences between the rates. This is due to different interpolation formulas which slightly differ since there is no measurement at low energy (see the convincing plot p. 58 of Angulo et al. (1999)).

^{15}N$(p,\gamma)^{16}$O: For the reaction which governs the efficiency of the NO-part of the CNO bi-cycle, N99, A98 and C88 adopt the use of S-factors at zero energy obtained by Rolfs & Rodney (1974). Due to differences in the interpolation formula, Fig. 2 reveals enhanced rates of $+15\%$ in N99 with respect to C88 or A98.

^{16}O$(p,\gamma)^{17}$F: At low energy the reaction which controls the generation of ν_{17_F}, the so-called fluorine solar neutrino, is based on data with large experimental errors. The adopted rate has the largest uncertainty among the CNO reactions. Though Table 1 gives for the three compilations about the same values for the S-factors, Fig. 2 shows large differences for the rates resulting from different analytical formulations. Beyond $T_6 \sim 10$, N99 and C88 are close (Angulo et al. 1999). The difference of -50% between A98 and C88 results of the used of the standard formulation of the non-resonant reaction rate with S-factors (Fowler et al. 1967).

^{17}O$(p,\alpha)^{14}$N: N99 and A98 use different analytical fits based on the measurements of Landré et al. (1989). They differ by -30%. Due to the discovery of a resonance at low energy (Landré et al. *loc. cit.*), the analytical fit of C88 is in error by more than two order of magnitude. For the models computed with C88 we have used the rates derived from the Landré et al.'s analytical fit, as recommended by A98.

Summary. With respect to C88, many reaction rates, principally ^{3}He$(^3$He$,2p)^4$He, are lowered in N99 and also, but to a lesser extent, in A98. One can expect that this will lead to calibrated

solar models with central cores with *larger* temperature. For the reactions of PP chains, with respect to C88, other important changes connected to the observable neutrino fluxes are the rates of the electronic capture ^{7}Be$(e^-, \nu_{7_{Be}}\gamma)^7$Li which is significantly diminished for $T_6 \lesssim 7$ in A98 and, for N99, the decrease of the rate of ^{7}Be$(p,\gamma)^8$B*. With respect to C88, the changes in N99 and A98 of the reaction rates of the CNO bi-cycle are not large enough to modify significantly the solar model.

3. The solar models

Basically the physics of the models is the same as in Morel et al. (1997).

Calibration of models. Each evolution is initialized with a homogeneous zero-age pre-main-sequence model in quasi-static gravitational contraction with the temperature at center $T_c \sim 0.5$ MK, i.e. close to the onset of the deuteron burning. The models are calibrated within a relative accuracy better than 10^{-4} by adjusting: the ratio l/H_p of the mixing-length to the pressure scale height, the initial mass fraction X_i of hydrogen and the initial mass fraction $(Z/X)_i$ of heavy element to hydrogen in order that, at present day, the solar models have the luminosity $L_\odot = 3.846\,10^{33}$ erg s^{-1} (Guenther et al. 1992), the radius $R_\odot = 6.9599\,10^{10}$ cm (Guenther et al. *loc. cit.*) and the mass fraction of heavy element to hydrogen $(Z/X)_\odot = 0.0245$ (Grevesse & Noels 1993). We used a time of evolution $t_{ev} = 4600$ My, an intermediate value between the meteoritic age $t_{\odot m} = 4530 \pm 40$ My of the Sun[1] (Guenther 1989) and its helioseismic value $t_{\odot h} = 4660 \pm 100$ My derived by Dziembowski et al. (1998). The zero age main-sequence (ZAMS) is defined as the time where nuclear reactions dominate gravitation as the primary energy source by more than 50% (Guenther et al. *loc. cit.*). The mass of the Sun is assumed to be $M_\odot = 1.9891\,10^{33}$ g (Cohen & Taylor 1986).

Nuclear and diffusion network. The general nuclear network we used contains the following species: ^{1}H , ^{2}H , ^{3}He , ^{4}He , ^{7}Li , ^{7}Be , ^{9}Be , ^{12}C , ^{13}C , ^{14}N , ^{15}N , ^{16}O , ^{17}O and Ex ; Ex is an "Extra" fictitious mean non-CNO heavy element with atomic mass 28 and charge 13 (Ex $\sim$ ^{28}Al) which complements the mixture i.e., $X_{Ex} = 1 - \sum_{i=^1H}^{^{17}O} X_i$ with X_i as the mass fraction of the species labeled with $i = ^1$H$, \ldots, ^{17}$O. With respect to time, due to microscopic diffusion processes, the abundances of heavy elements are enhanced toward the center; Ex mimics that enhancement for the non CNO metals which contribute to changes of Z, then to opacity variations but neither to nuclear energy generation nor to nucleosynthesis. To compute the depletion of ^{9}Be , we have added, to the nuclear network given Sect. 2, the most efficient reactions of ^{9}Be burning: ^{9}Be$(p,d)2\,^4$He and ^{9}Be$(\alpha,n)^{12}$C. The life time of the neutron,

---

namely 888 s (Barnett et al. 1996), is smaller by more than thirteen orders of magnitude than the evolutionary time scale of the Sun's main-sequence pp reaction. Therefore, for the calculations, the last reaction is rewritten $^9\text{Be}(\alpha, e^- p \bar{\nu}_{9\text{Be}})^{12}\text{C}$. The weak screening of Salpeter (1954) is used. It is a very good approximation of the exact solution of the Schrödinger equation for the fundamental pp reaction (Bahcall et al. 1998a).

The protosolar initial isotopic ratios (in number) for hydrogen and helium are respectively taken as $^2\text{H}/^1\text{H} = 3.01\,10^{-5}$, $^3\text{He}/^4\text{He} = 1.1\,10^{-4}$ (Gautier & Morel 1997). The initial ratios between the heavy elements within Z are set to their photospheric present day values, namely (in number) C: 0.24551, N: 0.06458 and O: 0.51295 (Grevesse & Noels 1993) then, for the complement Ex: 0.17696. The initial isotopic ratios are derived from the abundances of nuclides (Anders & Grevesse 1989): $^{13}\text{C}/^{12}\text{C} = 1.11\,10^{-3}$, $^{15}\text{N}/^{14}\text{N} = 4.25\,10^{-3}$, $^{17}\text{O}/^{16}\text{O} = 3.81\,10^{-4}$. We have used the meteoritic values (Grevesse & Sauval 1998) for the initial abundances in dex, (H $\equiv$ 12), of Li and Be :

$$\left[\frac{\text{Li}}{\text{H}}\right] = 3.31 \pm 0.04, \ \left[\frac{\text{Be}}{\text{H}}\right] = 1.42 \pm 0.04.$$

For the calculations of depletions, the lithium is assumed to be in its most abundant isotope ^7Li form, similarly beryllium is assumed to be ^9Be . Neither the meteoritic abundance nor the nuclide isotopic ratio of ^7Be are known, due to numerical constraints the protosolar abundance of ^7Be was somehow arbitrarily taken to a very low, but non zero value, namely $[^7\text{Be}/^1\text{H}] = -3.58$ dex. The initial abundance of each isotope is derived from isotopic ratios and initial values of $X \equiv {}^1\text{H} + {}^2\text{H}$, $Y \equiv {}^3\text{He} + {}^4\text{He}$ and Z/X as inferred by the calibration process in order to fulfill the basic relationship $X + Y + Z \equiv 1$.

Microscopic diffusion is described by the simplified formalism of Michaud & Proffitt (1993) with each of the heavy elements as a trace element.

Equation of state, opacities, convection and atmosphere. We have used the OPAL equation of state (Rogers et al. 1996) and opacities (Iglesias & Rogers 1996) for the solar mixture of Grevesse & Noels (1993) complemented, at low temperatures, respectively by the MHD equation of state (Däppen 1996) and Alexander & Ferguson (1994) opacities. The interpolations of opacities are made with the v9 birational spline package of G. Houdek (Houdek & Rogl 1996; Houdek 1998).

In the convection zones the temperature gradient is computed according to the standard mixing-length theory. The mixing-length is defined as $l \equiv \alpha H_\text{p}$, where H_p is the pressure scale height. The convection zones are mixed via a strong turbulent diffusion coefficient, which produces a homogeneous composition.

The atmosphere is restored using a $T(\tau)$ law derived from an atmosphere model of the Sun computed by van't Veer (1998) with the Kurucz's (1991) ATLAS12 package. The connection with the envelope is made at the Rosseland optical depth $\tau_\text{b} = 20$ (Morel et al. 1994), where the diffusion approximation for radiative transfer becomes valid. A smooth connection of the gradients is insured between the uppermost layers of the envelope and the optically thick convective part of the atmosphere. The radius $R_\star$ of any model is taken at the optical depth $\tau_\star \simeq 0.54$ where $T(\tau_\star) = T_\text{eff}$; the mass of the star $M_\star$, is defined as the mass enclosed in the sphere of radius $R_\star$. The external boundary is located at the optical depth $\tau_\text{ext} = 10^{-4}$, where the density is fixed to its value in the atmosphere model $\rho(\tau_\text{ext}) = 3.55\,10^{-9}\,\text{g cm}^{-3}$, that corresponds roughly to the temperature minimum in the solar chromosphere.

Numerics. The models have been computed using the CESAM code (Morel 1997). The numerical schemes are fully implicit and their accuracy is first order for the time and third order for the space. For numerical performance and algorithmic constraints the analytical expressions of reaction rates are tabulated with respect to temperature for the range $0.5 \leq T_6 \leq 20$ and interpolated with a relative accuracy better than 10^{-5}. Each evolution needs about 90 models. Typically 600 mass shell are used along the evolution, it increases up to 2100 for the models used in seismological analysis.

p-mode and g-mode oscillation calculations. The frequencies of linear, adiabatic, global acoustic modes of the solar models have been computed for degrees $\ell = 0$ to $\ell = 150$ and have been compared to the observations. The characteristic low degree p-mode frequency differences $\Delta\nu_{n,\ell} = \nu_{n,\ell} - \nu_{n-1,\ell+2}$ for $\ell = 0$ and $\ell = 1$, which provide information on the properties of the solar core, have been fitted by linear regressions with respect to n:

$$\Delta\nu_{n,\ell} = \delta\nu_{n,\ell} + S_\ell(n - n_0), \ n_0 = 21, \ \ell = 0, 1,$$

both for the observations and the theoretical frequencies. For the gravity modes which have not yet been observed, we give the characteristic asymptotic spacing period P_0 according to Provost & Berthomieu (1986).

4. Comparison of models

Table 2 gives the global properties of models and Fig. 3 exhibits the profiles, with respect to radius, of the most important variables for the internal structure namely, density, temperature, opacity, helium and heavy element contents.

4.1. Chemical composition

The changes in chemical composition directly result from changes of thermonuclear reaction rates but also, in a more intricate way, from changes in microscopic diffusion coefficients which are sensitive to the temperature and density, and to chemical composition, pressure, temperature and density gradients.

Changes at the surface and in the envelope. For the three models N99, A98 and C88, Table 2 shows that the expected photospheric abundances of helium are slightly reduced and remain compatible with the range of observed values. As known (Basu
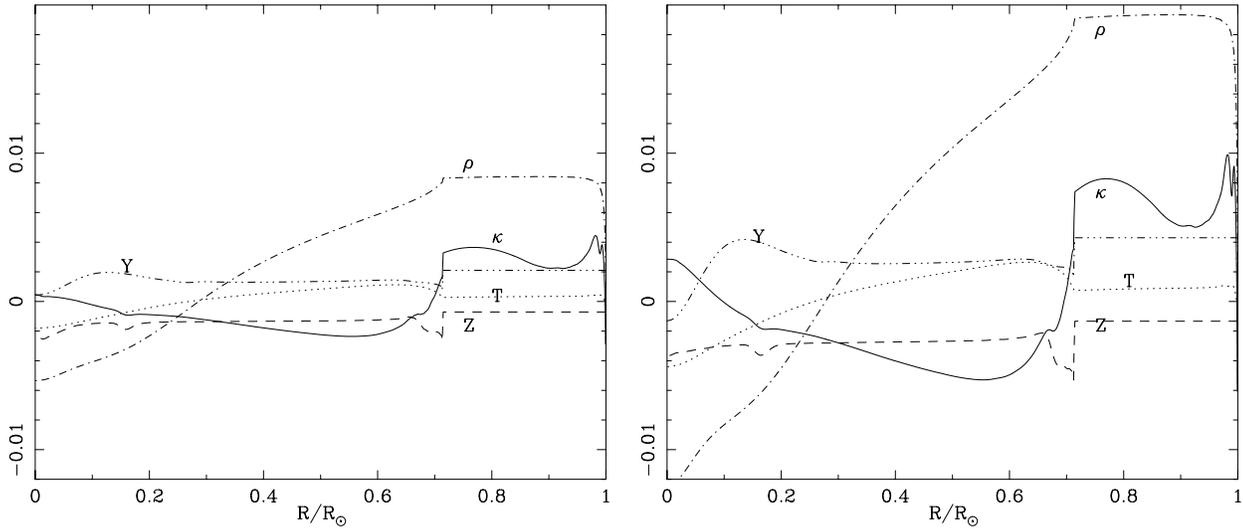
Fig. 3. Relative differences in opacity κ (full), heavy element Z (dashed), density ρ (dot-dash-dot-dash), temperature T (dotted) and helium content Y (dash-dot-dot-dash) for the calibrated models A98 (left) and C88 (right), with respect to model N99.
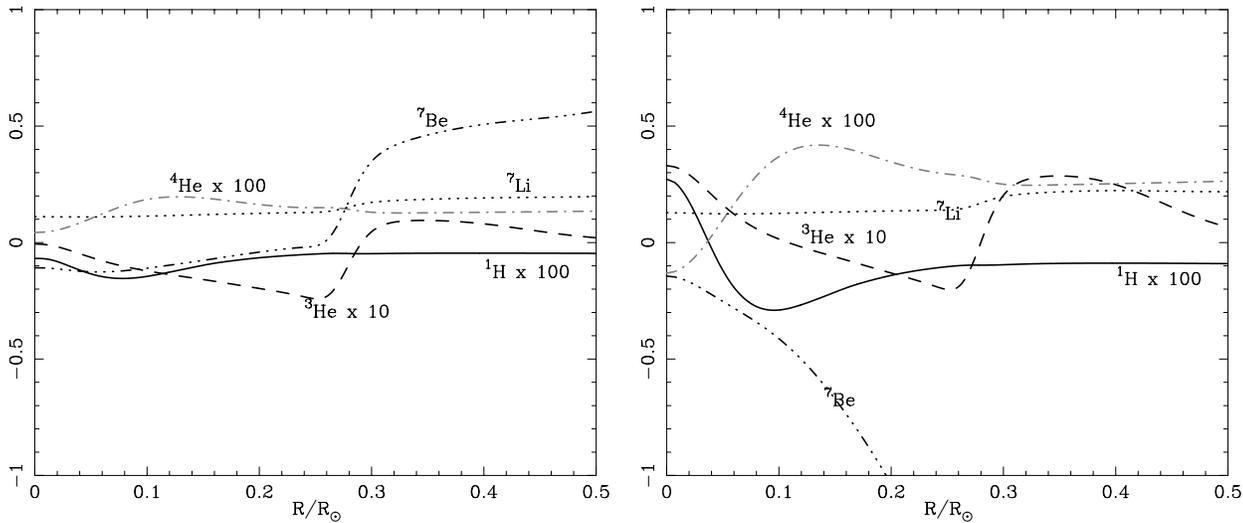

Fig. 4. Relative differences of abundances with respect to model N99, for models A98 (left) and C88 (right) for PP species: ^{1}H $\times$ 100 (full), ^{3}He $\times$ 10 (dashed), ^{4}He $\times$ 100 (dash-dot-dash), ^{7}Li (dotted), ^{7}Be (dash-dot-dot-dash).

1997b), the amount of photospheric "observed" helium derived from inversion of helioseismic data is more sensitive to the equation of state than the amount of photospheric "predicted" helium derived from calibrated solar models. Indeed we have calibrated a solar model[2] using C88 thermonuclear reaction rates and the MHD (Däppen 1996) equation of state instead of OPAL and obtained a photospheric helium content $Y_s = 0.246$ which is the value derived from inversion using the MHD equation of state (Basu & Antia 1995).

Though the ^{7}Li surface depletion is increased with the use of the enhanced rate of ^{7}Li$(p, \alpha)^4$He adopted by N99, the predicted abundance is still very far from the observed value. The differences are likely consequences of the lack, in standard solar models, of mixing generated by the shear at the level of

the tachocline (see e.g. Gough et al. 1996, Brun et al. 1999). It smoothes the chemical composition gradients and reduces the microscopic diffusion efficiency (Basu 1997a) immediately beneath the convection zone. According to the new observations (Grevesse & Sauval 1998), the predicted photospheric depletion of beryllium is tiny. The predictions for the surface isotopic ratios $(^3$He$/^4$He$)_s$ by the three models are all within the interval of accuracy given by the observations.

Changes in the core. The solar core is the innermost part where the nuclear energy generation is efficient. It extends from the center to about $R_c \simeq 0.4R_\odot$ slightly beyond the ^{3}He peak located around $0.3R_\odot$. Owing to the lower efficiency of PP reactions, see Sect. 2, the temperature, the density, the amount of helium and the sound velocity at center of *calibrated* mod-
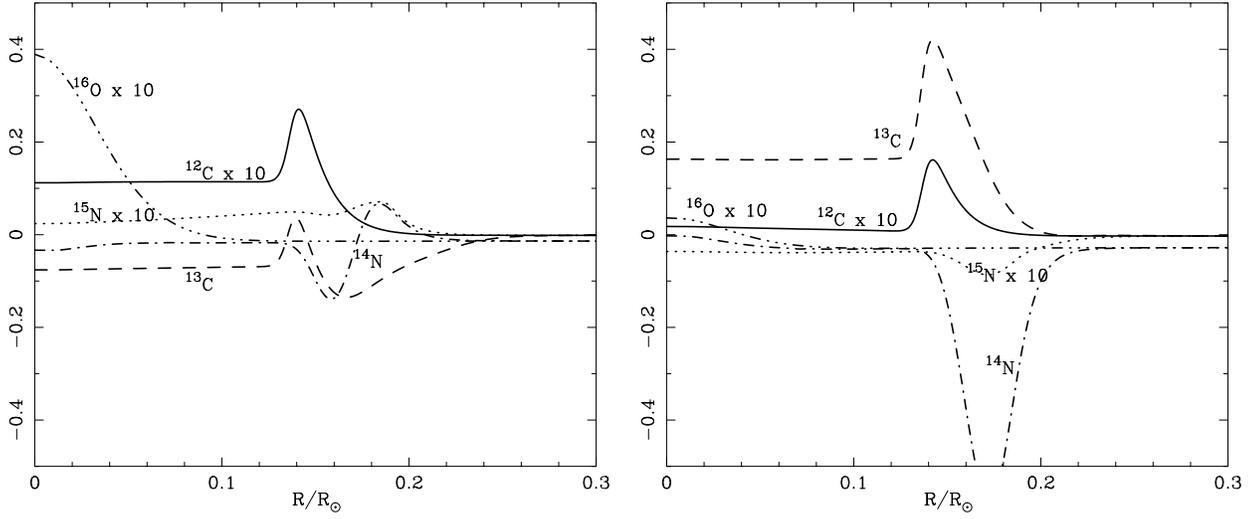
---

[2] Not analyzed here for sake of briefness.

Fig. 5. Same as Fig. 4 for the CNO species: ^{12}C $\times$ 10 (full), ^{13}C (dashed), ^{14}N (dash-dot-dash-dot), ^{15}N $\times$ 10 (dotted), ^{16}O $\times$ 10 (dash-dot-dot-dash).

Table 2. Comparison of global characteristics of solar models computed with the thermonuclear reaction rates of respectively Angulo et al. (1999, N99), Adelberger et al. (1998, A98) and Caughlan & Fowler (1988, C88) compilations. The first four rows give the initial values of Y_i (*resp.* Z_i) the mass fraction of helium (*resp.* heavy element), $(Z/X)_i$ the mass fraction of heavy element to hydrogen, α the mixing-length parameter. $^7\text{Li}_{sz}$ (*resp.* $^9\text{Be}_{sz}$) and $^7\text{Li}_s$ (*resp.* $^9\text{Be}_s$) respectively are the surface depletions in dex (H $\equiv$ 12) of ^{7}Li (*resp.* ^{9}Be) at zero-age main sequence and currently. All other items are for present day. The surface isotopic ratio $(^3\text{He}/^4\text{He})_s$ is in unit of 10^{-4}; Y_s, Z_s respectively are the surface mass fraction of helium and heavy element; R_{CZ} is the radius, in solar units, at the bottom of the convection zone; T_c, ρ_c, Y_c and Z_c are the central values respectively of, the temperature in units of 10^7K, the density in g cm^{-3}, the mass fraction, of helium and heavy element. $\delta\nu_{02}$ and $\delta\nu_{13}$ are the values, in μHz, of the frequency differences between the radial p-modes of degree $\ell = 0$–2 and $\ell = 1$–3. P_0 is the characteristic spacing period of g-modes in minutes.

	N99	A98	C88	Observed values
Y_i	0.2723	0.2726	0.2729	
Z_i	0.0197	0.0197	0.0196	
$(Z/X)_i$	0.0278	0.0278	0.0277	
α	1.924	1.931	1.941	
$^7\text{Li}_{sz}$	2.26	2.38	2.37	
$^9\text{Be}_{sz}$	1.42	1.42	1.42	
$^7\text{Li}_s$	2.18	2.30	2.29	1.10 ± 0.10, Grevesse & Sauval (1998)
$^9\text{Be}_s$	1.35	1.35	1.353	1.40 ± 0.09, Grevesse & Sauval (1998)
$(^3\text{He}/^4\text{He})_s$	4.34	4.32	4.32	4.4 ± 0.4, Bodmer et al. (1995)
Y_s	0.2436	0.2442	0.2447	$0.232 - 0.249$, Basu (1997b)
Z_s	0.0181	0.0181	0.0181	
R_{CZ}	0.7138	0.7132	0.7124	0.713 ± 0.001, Basu & Antia (1995)
T_c	1.573	1.570	1.566	
ρ_c	153.8	153.0	151.9	
Y_c	0.6418	0.6420	0.6409	
Z_c	0.0210	0.0210	0.0210	
$\delta\nu_{02}$	9.21	9.18	9.16	$9.002 \pm 0.044 - 9.014 \pm 0.042$, from LOI/GOLF (see text)
$\delta\nu_{13}$	16.10	16.06	16.03	$15.884 \pm 0.034 - 15.711 \pm 0.071$, from LOI/GOLF (see text)
P_0	35.13	35.23	35.42	

els N99 and A98, are larger than in C88. As expected, Fig. 4 shows almost symmetrical profiles for the differences for ^{1}H and ^{4}He. Owing to the larger efficiency of the pp reaction in C88, larger values are obtained for the relative difference C88 minus N99 than for A98 minus N99. The typical features for the relative differences of abundances of ^{3}He are consequences

of the smaller reaction rates of N99 with respect to A98 and C88 of $^3\text{He}(^3\text{He}, 2p)^4\text{He}$. Beneath the ^{3}He peak, owing to the increase of the temperature, the amount of ^{3}He is smaller in C88 and A98 than in N99; it is the reverse beyond the peak. Though the same rate prevails in N99 and A98 for the ^{7}Be electronic capture, there is a non zero value for relative difference between
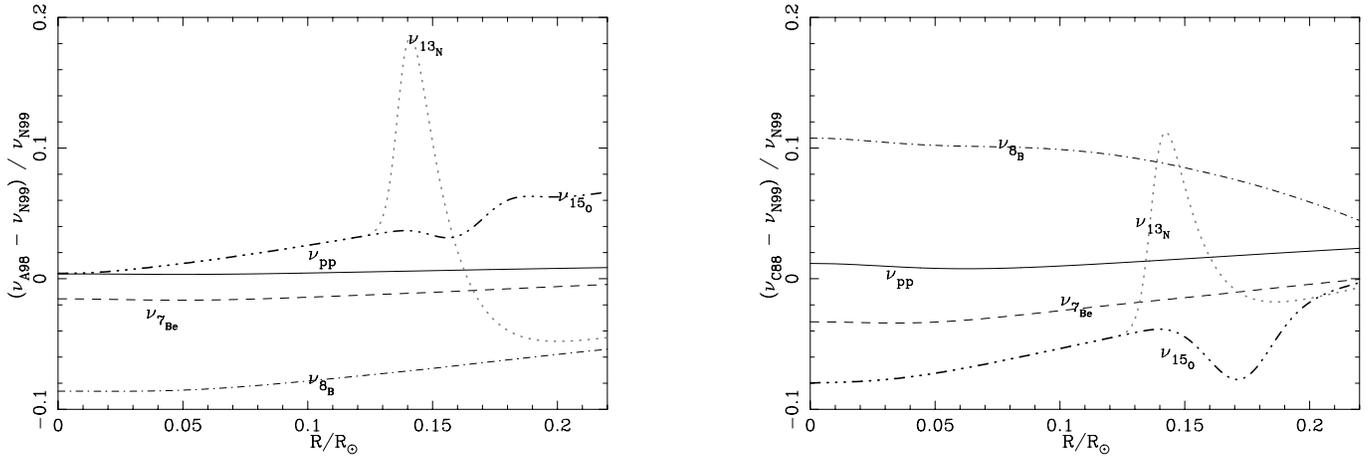
Fig. 6. Left panel: relative differences of neutrino rates generation, between models A98 and N99, for ν_{pp} (thin, full), ν_{7Be} (dashed), ν_{8B} (dot-dash-dot-dash), ν_{13N} (dotted), ν_{15O} (dash-dot-dot-dash). Right panel: the same between models C88 and N99

the ^{7}Be profiles of models N99 and A98, resulting in differences between the rates adopted for ^{3}He$(\alpha, \gamma)^7$Be.

Fig. 5 exhibits large differences in the abundances of ^{16}O for A98 and C88 with respect to N99 despite the fact that the rates of the reactions of ^{16}O burning are close. In fact, these differences result from changes of rates of ^{15}N burning which creates ^{16}O . For ^{12}C and ^{14}N , around $0.18R_\odot$, effects of changes of nuclear reaction rates are magnified by the large gradients of that species. There, Fig. 3 reveals, on Z profiles, small bumps due to the magnification by large gradients of variations in chemical composition caused by the changes of thermonuclear reaction rates.

4.2. Thickness of the convection zone

For radius $R \gtrsim 0.4R_\odot$, i.e. in the envelope, Fig. 3 shows that the opacity profiles are close within $\pm 0.4\%$ for models N99 and A98. The thickness of the convection zone is about the same in N99 and A98, and close, within the error bars (see Table 2), to the observed value. It is slightly larger for model C88. That difference is due to the increase of the radiative temperature gradient resulting from the higher value of the opacity. The differences of temperature between N99 and A98 being small, the changes in opacity are mainly due to the variations of density. The relative opacity differences amount to $\pm 1\%$ between C88 and N99.

4.3. Neutrinos

Table 3 gives the predicted neutrino fluxes at earth level and the expected fluxes for the three neutrino experiments namely, chlorine (e.g. Davis 1994), gallium (e.g. Hampel et al. 1999) and Kamiokande (e.g. Fukuda et al. 1996), computed according to Berthomieu et al. (1993). The gallium and chlorine absorption cross sections have been taken respectively from Bahcall (1997) and Bahcall et al. (1996). The hep flux which may be important (e.g. Bahcall & Krastev 1998, Fiorentini et al. 1998) in the neu-

Table 3. The same as Table 2 for the neutrino fluxes. Using the comprehensive symbols, defined Sect. 2, ν_{pp}, ν_{pep}, ν_{7Be}, ν_{8B}, ν_{13N}, ν_{15O}, ν_{17F} are, at earth level, the number cm^{-2} s^{-1} of neutrinos of each kind. Φ_{Ga} and Φ_{Cl} in SNU and Φ_{Ka} in events day^{-1}, are the expected fluxes for the three neutrino experiments namely gallium, chlorine and Kamiokande (see text). The observed values for Φ_{Ga}, Φ_{Cl} and Φ_{Ka} are respectively from Hampel et al. (1999), Davis (1994) and Fukuda et al. (1996).

	N99	A98	C88	Observed values
ν_{pp}	$5.91\,10^{10}$	$5.92\,10^{10}$	$5.94\,10^{10}$	
ν_{pep}	$1.40\,10^8$	$1.40\,10^8$	$1.48\,10^8$	
ν_{7Be}	$4.90\,10^9$	$4.80\,10^9$	$4.71\,10^9$	
ν_{8B}	$5.68\,10^6$	$5.17\,10^6$	$6.19\,10^6$	
ν_{13N}	$5.73\,10^8$	$5.77\,10^8$	$5.34\,10^8$	
ν_{15O}	$4.96\,10^8$	$5.01\,10^8$	$4.57\,10^8$	
ν_{17F}	$6.41\,10^6$	$3.15\,10^6$	$5.74\,10^6$	
Φ_{Ga}	130.1	128.4	129.8	$77.75 \pm 6.2^{+4.3}_{-4.7}$
Φ_{Cl}	8.31	7.71	8.82	2.55 ± 0.25
Φ_{Ka}	0.61	0.55	0.66	0.29 ± 0.02

trino spectrum measurements by the SuperKamiokande, SNO and Icarus experiments is not listed. With respect to C88, due to hotter core, ν_{7Be} and CNO neutrino fluxes are enhanced in A98 and N99 and, as expected, ν_{pp} is slightly reduced.

Despite larger temperatures in the core, we obtained, for the models A98 and N99 with respect to the model C88, the expected decreases of the ν_{8B} boron neutrino fluxes owing to their reduced rate of the reaction ^{7}Be$(p, \gamma)^8$B*. The introduction of N99 reaction rates relative to A98 induces an increase of $+10\%$ of ν_{8B}. The effect is significant on the flux measured by the chlorine and Kamiokande experiments. Note that Table 3 reveals that the neutrino fluxes at earth level for A98 are very similar those given Table 1 in Bahcall et al. (1998b). They differ only by a few percent for ν_{17F} owing to the large abundance of ^{16}O resulting from the great efficiency of ^{15}N burning
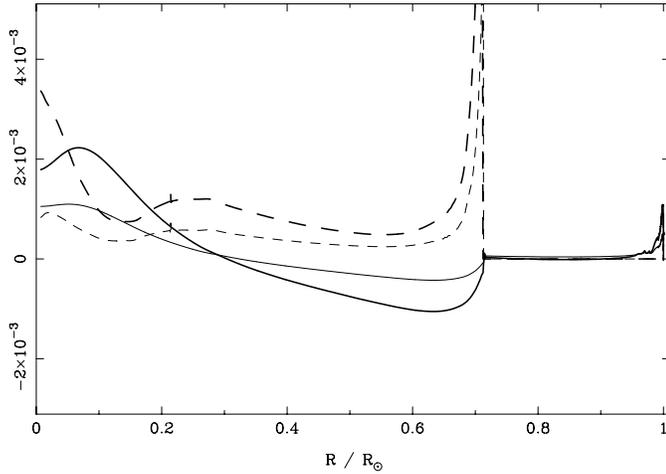
Fig. 7. Relative frequency differences of sound speed (full) and square of Brunt-Väisälä frequency divided by 10 (dashed) between N99 (thick) and C88, and A98 (thin) and C88.
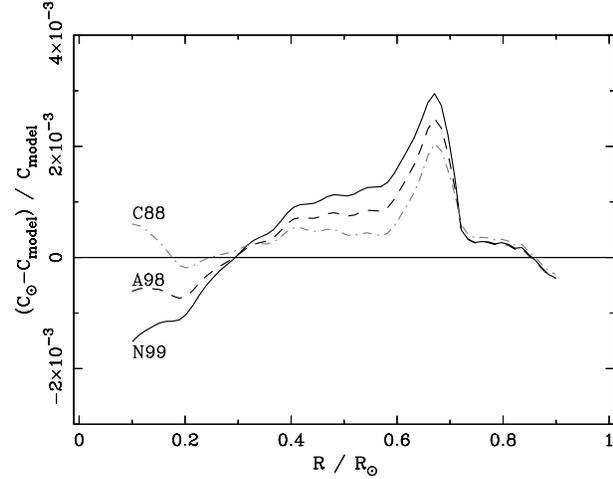

Fig. 9. Relative difference in sound velocity between the Sun and the calibrated models N99 (full), A98 (dashed) and C88 (dot-dash-dot-dash).
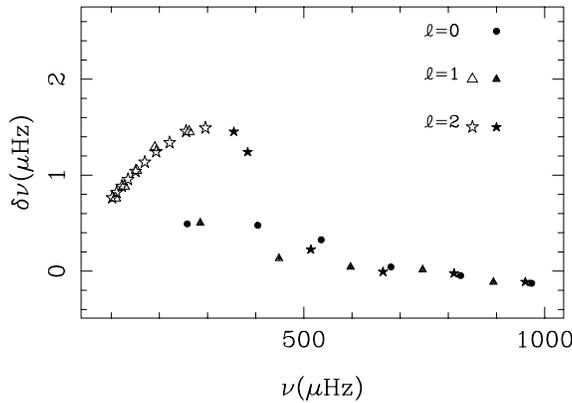

Fig. 8. Frequency differences (in μHz) in the low frequency range between N99 and C88 for modes of degree $\ell = 0$, 1, 2. Open symbols denote g-modes and, full symbols, f-modes and p-modes.

which about doubles the fraction of termination of the NO part of the CNO bi-cycle. Despite the fact that the two stellar evolution programs are entirely independent of each other, when the same nuclear reaction rates are used (A98), the most important neutrino fluxes ν_{pp}, ν_{pep}, ν_{7Be}, ν_{8B}, ν_{13N}, and ν_{15O} all agree to better than 1%.

4.4. Seismological comparison

The seismic properties of the solar model are mainly related to the profile of sound-speed (*resp.* Brunt-Väisälä frequency) as far as p-modes (*resp.* g-modes) are concerned. Fig. 7 shows that the models N99 and, to a lesser extend A98, compared to C88, have a larger sound speed in the central core below 0.3 solar radius by +0.2% (*resp.* +0.1%), and a smaller one by -0.1% (*resp.* -0.05%) just below the convection zone. Table 2 shows a small increase of small low degree differences $\delta\nu_{02}$ and $\delta\nu_{13}$, as defined in Sect. 3 in relation to the difference of sound speed in the solar core. There the relative differences in

the Brunt-Väisälä frequency between models N99 and C88 are larger by a few percent, i.e. one order of magnitude larger than the sound speed differences. The increase of the Brunt-Väisälä frequency leads to a -1% smaller value of P_0, the characteristic spacing period of g-modes. The differences between A98 and C88 are three times smaller. This change in Brunt-Väisälä frequency influences greatly the low frequency modes for frequency less than 1 mHz, i.e. the low radial order p-modes, the f- and g-modes. Consequently the frequency differences of the low degree p-modes between models N99 and C88 vary from $-0.1\,\mu$Hz to $-0.25\,\mu$Hz when the frequency increases from 1 mHz to 5 mHz, with a minimum value of $-0.5\,\mu$Hz around 2 mHz. The normalized frequencies differences for p-modes of degree $\ell = 3$ to $\ell = 150$ are negative and change by less than $-1\,\mu$Hz in the observed range. As expected, the change of nuclear reaction rates do not modify the frequency of oscillation of degree larger than 70.

Fig. 8 shows the frequencies differences in low frequency range between N99 and A98 and Table 4 gives the frequencies of g- and p-modes for $\ell = 0$ to $\ell = 2$ in the same frequency range. In the low frequency range $400\,\mu$Hz – 1 mHz, it appears that the p-mode frequencies are changed by less than $0.5\,\mu$Hz between N99 and C88, i.e. by less than $+0.1\%$, with an larger effect at lower frequency. Below $200\,\mu$Hz, the oscillations are gravity modes with an asymptotic behavior, and the relative period differences are almost proportional to P_0 given in Table 4 (see Provost et al. 1998 for details). Between 200 to $400\,\mu$Hz, the oscillations are gravity modes, or f- and p1-modes and they are more influenced by the change of the Brunt-Väisälä frequency in the solar core, induced by changes in nuclear reactions, except the p1-modes for $\ell = 0$ and $\ell = 1$. Frequencies shifts are much larger, of the order of 1 to $1.5\,\mu$Hz, when the frequency varies from $200\,\mu$Hz to $400\,\mu$Hz, i.e. about 1%, when comparing the models N99 and C88.

In the range $0.1\,R_\odot \lesssim R \lesssim 0.9\,R_\odot$ where the inversions of the helioseismic data are reliable, the sound speed of the three

Table 4. Frequency of g-modes and p-modes in the range $100\,\mu$Hz–$2\,$mHz. $\mathcal{T}$ is the type of the mode labelled by the radial order.

ℓ	C88	N99	$\mathcal{T}$	ℓ	C88	N99	$\mathcal{T}$
0	257.82	258.31	p1	2	101.88	102.64	g10
	404.32	404.79	p2		111.07	111.88	g9
	535.98	536.30	p3		121.91	122.80	g8
	680.67	680.71	p4		134.87	135.82	g7
	825.56	825.52	p5		150.51	151.55	g6
	972.95	972.82	p6		169.69	170.83	g5
	1118.36	1118.15	p7		193.24	194.49	g4
	1263.78	1263.60	p8		221.23	222.57	g3
	1407.86	1407.58	p9		255.22	256.67	g2
	1548.78	1548.51	p10		295.44	296.93	g1
	1687.12	1686.81	p11		354.60	356.06	f
	1822.51	1822.14	p12		383.36	384.60	p1
	1957.79	1957.44	p13		514.35	514.58	p2
					664.33	664.33	p3
1	108.55	109.31	g5		811.77	811.75	p4
	127.04	127.93	g4		959.86	959.75	p5
	152.45	153.50	g3		1105.18	1105.01	p6
	190.56	191.85	g2		1250.78	1250.60	p7
	261.62	263.07	g1		1394.73	1394.46	p8
	284.77	285.27	p1		1536.06	1535.80	p9
	448.34	448.48	p2		1674.78	1674.44	p10
	596.90	596.95	p3		1810.37	1810.01	p11
	746.65	746.66	p4		1946.00	1945.63	p12
	893.71	893.60	p5				
	1039.63	1039.52	p6				
	1185.68	1185.47	p7				
	1329.80	1329.57	p8				
	1473.13	1472.88	p9				
	1612.86	1612.53	p10				
	1749.57	1749.25	p11				
	1885.34	1884.94	p12				

models has been compared with the seismic sound speed experimental results of Turck-Chièze et al. (1997). Fig. 9 shows that the relative differences are below a few 10^{-3}. The discrepancy between the Sun and the models is larger for model N99 with sound speed too small just below the convection zone and too large in the core. Table 2 shows that it is the same for the quantities $\delta\nu_{02}$ and $\delta\nu_{13}$ of the models compared to the corresponding observed values $\delta\nu_{n,\ell}$ derived from GOLF (Grec et al. 1997) and VIRGO/LOI (Fröhlich et al. 1997) observations on SoHO.

5. Discussion and conclusions

We have compared the structure, the neutrino fluxes, the chemical composition profiles and the helioseismological properties of calibrated standard solar models computed with the adopted nuclear reaction rates of the European compilation NACRE (Angulo et al. 1999) with those of calibrated solar models computed with the nuclear reaction rates of Caughlan & Fowler (1988) and Adelberger et al. (1998).

Roughly speaking, the thermonuclear reaction rates of PP chains adopted by NACRE and, but to a lesser extend, by Adelberger et al., are slightly less efficient than those adopted by Caughlan & Fowler. The calibration generates models with cores of larger temperature, density, helium content and sound speed with the concomitant increase of the neutrino fluxes, except for ν_{pp} and ν_{8_B}; for this last one, the decrease is due to the smaller rate of the reaction $^7\text{Be}(p,\gamma)^8\text{B}^*$. Thus the predicted neutrino fluxes are reduced for the chlorine and Kamiokande experiments, but almost unchanged for gallium. For Kamiokande and chlorine, N99 predicts intermediate values between A98 and C88.

The introduction of the NACRE thermonuclear rates increases the discrepancy between predicted and observed sound velocity profiles between the Sun and the models, both below the convection zone and in the solar core. These relative differences, though at the level of a few thousandths, are smaller for the model computed with the reaction rates of Caughlan & Fowler, the increase is $\sim +0.5\%$ for C98 and $\sim +1\%$ for N99. The radius at the base of the solar convection zone is in good agreement with the observed value for all models.

Though NACRE adopts an enhanced rate for the reaction of lithium burning $^7\text{Li}(p,\alpha)^4\text{He}$, the predicted depletion of photospheric lithium remains too small to fit the observed value.

The differences between calibrated solar models computed with the adopted thermonuclear reaction rates of the two new compilations are rather small. It is not really possible to make a choice between them. From an increase in the accuracy of the observed p-mode frequencies and hopefully from detection of g-modes, one can expect to improve our knowledge on the stratification of the solar core with the goal to validate, in the low energy regime, the thermonuclear reaction rates and their concomitant neutrino generation.

References

Adelberger E.G., Austin S.M., Bahcall J.N., et al., 1998, Rev. Mod. Phys. 70, 4, 1265

Alexander D.R., Fergusson J.W., 1994, ApJ 437, 879

Angulo C., Arnould M., Rayet M., (NACRE collaboration), 1999, Nuclear Physics A 656, 1, http://pntpm.ulb.ac.be/Nacre/nacre.htm

Anders E., Grevesse N., 1989, Geochimica et Cosmochimica Acta 53, 197

Arnould M., Goriely S., Jorissen A., 1999, A&A 347, 572

Bahcall J.N., Fowler W.A., Iben I.Jr., Sears R.L., 1963, ApJ 137, 344

Bahcall J.N., Ulrich R.K., 1988, Rev. Mod. Phys. 60, 297

Bahcall J.N., 1989, Neutrino Astrophysics. Cambridge University Press

Bahcall J.N., Pinsonneault M.H., 1992a, Rev. Mod. Phys. 60, 297

Bahcall J.N., Pinsonneault M.H., 1992b, ApJ 395, L119

Bahcall J.N., 1993, Solar Neutrinos: What We Have Learned. In: Roxburg I.W., Masnou J.-L. (eds.) Physical Processes in Astrophysics. Proceedings of a Meeting in Honour of Evry Schatzman. Lecture Notes in Physics, Springer-Verlag, Berlin-Heidelberg, 1995, p. 19

Bahcall J.N., Pinsonneault M.H., Wasserburg G.J., 1995, Rev. Mod. Phys. 67, 781

Bahcall J.N., Lisi E., Alburger D.E., et al., 1996, Phys. Rev. C 54, 411

Bahcall J.N., 1997, Phys. Rev. C 56, 3391

Bahcall J.N., Chen X., Kamionkowski M., 1998a, Phys. Rev. C 57, 2756

Bahcall J.N., Basu S., Pinsonneault M.H., 1998b, Phys. Lett. B 433, 1

Bahcall J.N., Krastev P.I., 1998, Phys. Lett. B 436, 243

Barnett R.M., Carone C.D., Groom D.E., et al., 1996, Phys. Rev. D. 54, 1

Basu S., Antia H.M., 1995, MNRAS 276, 1402

Basu S., 1997a, MNRAS 288, 572

Basu S., 1997b, The seismic Sun. In: Provost J., Schmider F.X. (eds.) Sounding solar and stellar interiors. IAU Syposium 181, Kluwer Academic Publishers, p. 137

Berthomieu G., Provost J., Morel P., Lebreton Y., 1993, A&A 268, 775

Berthomieu G., Provost J., Morel P., 1995, Neutrino capture rates predicted by standard solar models. In: Ulrich R.K., Rhodes E. J., Däppen W. (eds.) GONG94 Helio and Asteroseismology from earth and space. ASP Conf. Series 76, 109

Brun A.S., Turck-Chièze S., Morel P., 1998, ApJ 506,913

Brun A.S., Turck-Chièze S., Zahn J.P., 1999, ApJ in press, astro-ph/9906382

Bodmer R., Bochsler P., Geiss J., von Steiger R., Gloecker G., 1995, Space Sci. Rev. 72, 61

Caughlan G.R., Fowler W.A., 1988, Atomic Data and Nuclear Data Tables 40, 284

Chaboyer B., Demarque P., Pinsonneault M.H., 1995, ApJ 441, 865

Christensen-Dalsgaard J., Däppen W., Ajukov S.V.,1996, Sciences 272, 1286

Castellani V., Degl'Innocenti S., Fiorentini G., Lisia M., Ricci B., 1997, Phys. Rep. 281, 309

Clayton D.D., 1968, Principles of Stellar Evolution and Nucleosynthesis. Mc Graw–Hill

Cohen E.R., Taylor B.N., 1986, Codata Bulletin No. 63, Pergamon Press New York

Davis R. Jr., 1994, Prog. Part. Nucl. 32, 13

Däppen W., 1996, Bull. Astron. Soc. India 24, 151

Dziembowski W.A., Fiorentini G., Ricci. B., Sienkiewicz R., 1998, A&A in press, astro-ph/9809361

Fiorentini G., Berezinsky V., Deg'Innocenti S., Ricci B., 1998, astro-ph/9810083

Fowler W.A., Caughlan G.R., Zimmerman B.A., 1967, ARA&A 5, 523

Fröhlich C., Andersen B.N., Appourchaux T., et al., 1997, First results from VIRGO on SoHO. In: Provost J., Schmider F.X. (eds.) Sounding solar and stellar interiors. IAU Syposium 181, Kluwer Academic Publishers, 67

Fukuda Y., (Kamiokande Collaboration), 1996, Phys. Rev. Lett. 77, 1683

Gautier D., Morel P., 1997, A&A 323, L9

Gough D.O., Kosovichev A.G., Toomre J., et al., 1996, Sciences 272, 1296

Grec G., Turck-Chièze S., Lazrek M., et al., 1997, GOLF results: today's view on the solar modes. In: Provost J., Schmider F.X. (eds.) Sounding solar and stellar interiors. IAU Syposium 181, Kluwer Academic Publishers, 91

Grevesse N., Noels A., 1993, Cosmic Abundances of the Elements. In: Prantzos N., Vangioni-Flam E., Casse M. (eds.) Origin and Evolution of the Elements. Cambridge University Press, 14

Grevesse N., Sauval A.J., 1998, Standard Solar Composition. In: Frölich C., Huber M.C.E., Solanki S.K., Von Steiger R. (eds.) Solar Composition and its Evolution - from Core to Corona. ISSI workshop, Space Sciences Series of ISSI 5, 161

Guenther D.B., 1989, ApJ 339, 1156

Guenther D.B., Demarque P., Kim Y.C., Pinsonneault M.H., 1992, ApJ 387, 372

Hampel W., Handt J., Heusser G., (GALLEX collaboration), 1999, Phys. Lett. B 447, 127

Houdek G., Rogl J., 1996, Bull. Astr. Soc. India 24, 317

Houdek G., 1998, v9 opacities package taken from the WEb site ftp://solaris.tuwien.ac.at/incoming/

Iglesias C.A., Rogers F.J., 1996, ApJ 464, 943

Junker M., D'Alessandro A., Zavatarelli S., et al., 1998, Phys. Rev. C 57, 2700

Kurucz R.L., 1991, Stellar Atmospheres: Beyond Classical Models. In: Crivallery L., Hibeny I., Hammer D.G. (eds.) NATO ASI Series, Kluwer, Dordrecht

Landré V., Aguer P., Bogaert G., et al., 1989, Phys. Rev, C 40, 1972

Michaud G., Proffitt C.R., 1993, Particule Transport Process. In: Baglin A., Weiss W.W. (eds.) Inside the Stars. IAU Colloquium 137, ASP Conference Series Vol. 40, ASP, 246

Morel P., van't Veer C., Provost J., et al., 1994, A&A 286, 91

Morel P., 1997, A&AS 124, 597

Morel P., Provost J., Berthomieu G., 1997, A&A 327, 349

Morel P., Provost J., Berthomieu G., 1998, How solar models fit the SoHO observations? In: A. Wilson (ed.) SOHO6/GONG98: Structure and Dynamics of the Interior of the Sun and Sun-like Stars. ESA Publication SP-418, p. 499

Provost J., Berthomieu G., 1986, A&A 165, 218

Provost J., Berthomieu G., Morel P., 1998, Sensitivity of low frequency oscillations to updated solar models. In: Fröhlich C., Huber M.C.E., Solanki S., von Steiger R. (eds.) Solar composition and its evolution - From Core to Corona. Space Sci. Rev. 85, p. 117

Rogers F.J., Swenson F.J., Iglesias C.A., 1996, ApJ 456, 902

Reiter J., Walsh L., Weiss A., 1995, MNRAS 274, 899

Rolfs C., Rodney W.S., 1974, Nucl. Phys A 235, 450

Salpeter E.E., 1954, Australian J. Phys. 7, 373

Turch-Chièze S., Basu S., Brun S., et al., 1997, Solar Phys. 175, 247

vant't Veer C., 1998, private communication